Russian Geology and Geophysics © 2019, V.S. Sobolev IGM, Siberian Branch of the RAS
Vol. 60, No. 8, pp. 862–875, 2019 *DOI:10.15372/RGG2019062* *Geologiya i Geofizika*

Sources of Sulfur for Sulfide Mineralization in the Archean Rocks of the Sharyzhalgai Uplift of the Siberian Craton Basement (from Multi-Isotope Data)

S.V. Vysotskiy [a,c,] ✉, A.V. Ignat'ev [a], V.I. Levitskii [b], T.A. Velivetskaya [a], A.V. Aseeva [a,c], I.V. Levitskii [b], A.S. Mekhonoshin [b]

[a] *Far East Geological Institute, Far Eastern Branch of the Russian Academy of Sciences, pr. 100-letiya Vladivostoka 159, Vladivostok, 690022, Russia*

[b] *A.P. Vinogradov Institute of Geochemistry, Siberian Branch of the Russian Academy of Sciences, ul. Favorskogo 1a, Irkutsk, 664033, Russia*

[c] *Far Eastern Federal University, ul. Sukhanova 8, Vladivostok, 690950, Russia*

Received 15 January 2018; received in revised form 26 April 2018; accepted 15 June 2018

Abstract—We present results of study of sulfide ore occurrence in highly metamorphosed (granulite facies) Archean rocks of the Siberian craton basement. The host rocks and ore minerals are briefly described, and new data on the multiple sulfur isotope ($\delta^{33}S$, $\delta^{34}S$, $\Delta^{33}S$) composition of sulfides are presented. Application of high-resolution analytical methods enabling the assessment of the sulfur isotope behavior in situ made it possible to reveal mass-independent fractionation of sulfur isotopes in the rock samples. The isotopic composition of sulfur in the sulfides indicates its inflow from several sources, including the ancient Archean atmosphere, where primary sulfur has passed through a cycle of fractionation. Despite the high-gradient metamorphism, the subsequent ultrametamorphic and post-ultrametamorphic transformations accompanied by a change in the primary mineral composition of rocks and by chemogenic fractionation of sulfur, the signature of the sedimentary source of sulfur in sulfide ores has been well preserved. Analysis of the chemical composition of rocks and ore minerals and of sulfur isotopes has led to the conclusion that the studied rocks are metamorphosed Late Archean analogs of black shales and the sulfide mineralization is of stratiform pyrite type.

Keywords: sulfur isotopes, black shales, mass-independent fractionation, pyrite ores, Siberian craton, Sharyzhalgai marginal uplift

INTRODUCTION

A number of large sulfide ore deposits formed on the Earth throughout the Archean and Early Proterozoic. Elucidation of the sources of their sulfur and metals is of great importance for understanding their genesis. Data on the isotopic composition of sulfur are often invoked to establish its sources (Grinenko and Grinenko, 1974; Grichuk and Lein, 1991; Butler et al., 1998). The above studies were performed using the ratios of two most common sulfur isotopes (^{32}S and ^{34}S), although sulfur has four stable isotopes, ^{32}S, ^{33}S, ^{34}S, and ^{36}S, with their natural relative abundance of 95.02, 0.75, 4.21, and 0.02%, respectively. This was partly due to the limitations of analytical methods and also due to the clear correlation among the $\delta^{33}S$, $\delta^{34}S$, and $\delta^{36}S$ values (Hulston and Thode, 1965), called the mass-dependent fractionation (MDF) of sulfur isotopes. Fractionation of sulfur isotopes runs through kinetic isotope effects during biologic processes and a chemical exchange between different sulfides and between sulfides and sulfates. However, until recently it has been believed that measurement of $\delta^{33}S$ and $\delta^{36}S$ would yield no additional information (Johnston, 2011).

It was found, however, that MDF is often disturbed in the case of Archean and Early Proterozoic deposits. Deviation from MDF is called mass-independent fractionation of sulfur (MIF-S), and the deviation value is denoted $\Delta^{33}S‰$. It is believed that MIF-S is the result of photochemical reactions running in an anoxic atmosphere under ultraviolet radiation (Farquhar et al., 2000; Pavlov and Kasting, 2002; Farquhar and Wing, 2003; Bekker et al., 2004). At present, this viewpoint is predominant, although not the only one. Other possible variants of anomalous fractionation of isotopes are chemisorption reactions (Lasaga et al., 2008) or thermochemical sulfate reduction by amino acids (Watanabe et al., 2009), but there is still controversy as to whether these processes were relevant for mass-independent fractionation in Archean rocks (Farquhar et al., 2010; Golding et al., 2011; Roerdink et al., 2012).

Mass-independent fractionation of sulfur isotopes is a distinctive feature of Early Precambrian sedimentary rocks and reflects atmospheric processes at that time. In subsequent sulfur-involving geologic (igneous, metamorphic, and

✉ Corresponding author.
E-mail adress: vysotskiy@fegi.ru (S.V. Vysotskiy)

metasomatic) transformations, the nonzero values of $\Delta^{33}S$ are usually preserved even in the case of significant MDF, unless mixing processes dilute the $\Delta^{33}S$ signature to values below its detection limit. As a result, MIF-S is a chemically conserved tracer indicating that sulfur is involved in the ore formation. In this research we use multiple sulfur isotope composition to determine the sources of this element in the sulfides of the Cheremshanka pyrite ore occurrence in the Sharyzhalgai marginal uplift of the Siberian craton.

MATERIAL AND METHODS

Material for study was sampled during the prospecting and mapping performed by the Angarsk Geosurvey Expedition of the Irkutskgeologiya State Geological Enterprise in the late 1980–early 1990s. Drilling in the basin of the Srednyaya (Middle) Cheremshanka River, a right tributary of the Kitoi River, revealed veinlet-disseminated pyrite–pyrrhotite mineralization in the Cheremshanka Formation of the Sharyzhalgai granulite complex in the Sharyzhalgai (Cis-Sayan) marginal uplift.

Sampling was made from the cores of five prospecting/mapping boreholes up to 500 m in depth. Samples with sulfides (pyrite, pyrrhotite, chalcopyrite, etc.) in the form of dissemination, clusters, nests, thin veinlets, solid zones, and massive ores were used for isotope studies.

Analyses of rocks were carried out in the Chemical Analytical Laboratory of the Institute of Geochemistry, Irkutsk, using the following methods: X-ray fluorescence (major and trace elements—Ba, Sr, Zr, Nb, and Ta), "wet chemistry" and flame photometry (K, Na, Li, Rb, and Cs), quantitative emission spectroscopy (Ba, Sr, B, Be, F, Mo, W, Sn, La, Ce, Yb, Y, Zr, Cr, V, Ni, and Co), and atomic-absorption spectroscopy (Ca, Mg, Fe, Mn, Si, and Al). Each sample was analyzed by different methods. Table 1 presents the average contents obtained by methods with the lowest detection limits of elements. The detection limits are as follows: Na_2O and K_2O—0.01%; ppm: Li, Rb, and Cs—0.5–1 (flame photometry), Ba and S—2–3, B—1, Be—0.05, F—50, Mo and Sn—0.1, La, Ce, Nd, and Zr—5–15, Yb and Y—0.1–1.0, Pb, Zn, Cr, and V—1, Ni, Co, and Cu—0.5, Ag—0.01 (quantitative spectral method); Ba and Sr—1, Zr, Nb, and Ta—1-2 (X-ray fluorescence).

Analyses of minerals were made in the Laboratory of X-Ray Methods of the Analytical Center of the Far East Geological Institute, Vladivostok, using a JEOL JXA 8100 electron microprobe (Japan) with three wavelength-dispersive spectrometers and an INCA EMF spectrometer (England) with a MnK_α resolution of 137 eV at an accelerating voltage of 20 kV and a current of 1×10^{-8} A. In the point study of minerals, the material to be analyzed was 1 to 3 μm in size. Electron images were obtained by BSE scanning. Pure metals, glasses, and minerals analyzed by other methods and MAC standards were used as reference samples. Total Fe was taken as Fe^{2+}.

Sulfur isotope analyses were carried out in the Laboratory of Stable Isotopes of the Analytical Center of the Far East Geological Institute, Vladivostok, using the local laser method (Ignatiev et al., 2018). The sulfur isotope ratio was measured for isotopic masses of 127 ($^{32}SF_5^+$), 128 ($^{33}SF_5^+$), and 129 ($^{34}SF_5^+$) on an MAT-253 mass spectrometer in a three-beam mode. The measurement results, $\delta^{33}S$ and $\delta^{34}S$, ‰, are given relative to the VCDT International Standard. The accuracy of analyses of sulfide inclusions with a spatial resolution of ~100 μm is $\delta^{34}S \pm 0.20$‰ (1σ), $\delta^{33}S \pm 0.15$‰ (1σ), and $\Delta^{33}S \pm 0.05$‰.

GEOLOGIC SETTING

Geologic structure. The Sharyzhalgai (Cis-Sayan) marginal uplift (Grabkin and Mel'nikov, 1980; Rosen, 2003) comprises the main typical structures of the Precambrian continental crust: granite–greenstone and granulite–gneiss complexes (areas). Four large blocks are recognized within it: Bulun, Kitoi, Zhidoi, and Irkut (Grabkin and Mel'nikov, 1980; Mel'nikov, 2011), differing in rock composition, morphology, and evolution of large structures (Fig. 1). The Neoarchean Kitoi complex in the Kitoi block and the polychronous Neoarchean–Paleoproterozoic (2.5–1.8 Ga) Sharyzhalgai complex in the Zhidoi and Irkut blocks are composed of rocks of the granulite facies (Sal'nikova et al., 2007).

Starting from the 1960s, the lower Archean section of the Sharyazhalgai Group was separated (from bottom to top) into the Zhidoi, Zoga, and Cheremshanka Formations. According to the latest geological-mapping data (Galimova et

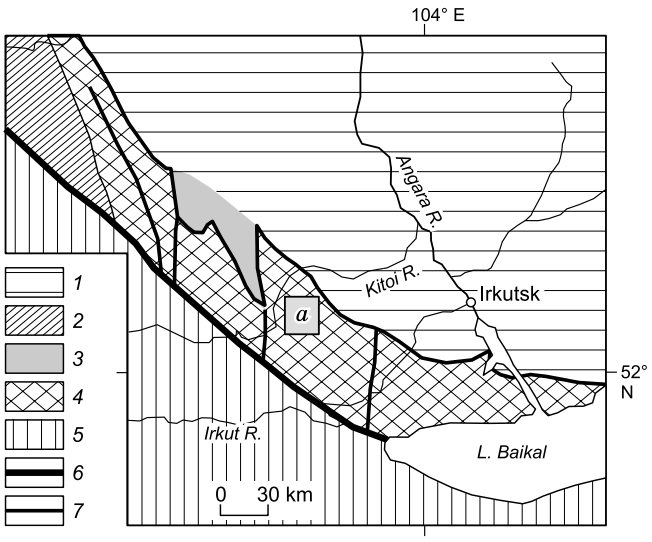

Fig. 1. Schematic geological map of the Sharyzhalgai marginal uplift of the Siberian craton. *1*, sedimentary cover of the Siberian craton; *2–4*, structures of the marginal uplift of the platform basement: *2*, Urik–Iya graben, *3*, Onot greenstone belt, *4*, Sharyzhalgai granulite–gneiss complex; *5*, terranes of the Central Asian Fold Belt; *6*, Main Sayan deep fault; *7*, other faults. *a*, Area of study of sulfur isotopes in sulfides of the Cheremshanka Formation of the Sharyzhalgai granulite complex.

Table 1. Chemical (wt.%) and trace-element (ppm) compositions of rocks

Component	1	2	3	4	5	6	7	8	9	10	11	12
	Kh1/15	Kh1/16	Kh1/37	Kh1/38b	Kh1/40	Kh10/4	Kh10/6	Kh1/28	Kh1/31b	Kh1/35	Kh11/7a	Kh5/2a
SiO_2	49.48	48.95	46.05	36.29	42.62	40.44	46.60	53.20	40.21	53.06	24.02	56.44
TiO_2	0.75	0.76	0.63	0.49	0.38	1.04	0.66	1.56	0.42	0.59	0.11	0.37
Al_2O_3	13.85	18.30	16.05	11.81	12.30	11.3	13.2	14.24	8.32	13.72	4.60	9.45
FeO	—	8.58	7.89	23.8	7.99	14.5	7.45	13.2	21.01	14.18	18.95	9.25
Fe_2O_3	12.2*	1.43	4.44	6.05	5.23	2.70	1.43	1.69	2.98	2.02	11.61	0.75
MnO	0.15	0.15	0.04	0.05	0.08	0.09	0.13	0.23	0.39	0.24	0.19	0.14
MgO	3.60	4.70	2.10	1.36	2.30	2.30	2.40	5.30	4.75	3.30	1.75	3.07
CaO	2.30	2.00	1.80	0.78	1.30	1.85	1.30	7.93	1.30	7.19	2.33	16.48
P_2O_5	0.07	0.12	0.10	0.05	0.10	0.08	0.07	0.15	0.12	0.10	0.07	0.08
K_2O	2.51	4.01	2.4	4.64	2.76	1.76	2.59	0.36	3.62	1.45	1.13	1.51
Na_2O	1.76	1.98	2.12	1.72	1.39	1.45	1.50	1.41	1.19	1.82	0.55	0.58
LOI	6.42	4.81	10.31	2.37	17.47	15.20	17.59	0.98	9.01	0.84	23.10	0.85
S	6.47	3.40	5.73	10.77	5.63	7.27	4.92	—	6.38	1.21	10.93	1.52
CO_2	0.37	0.52	0.53	—	0.58	0.24	0.44	—	0.43	—	0.95	—
Total	100.01	99.95	100.31	100.18	100.13	100.22	100.28	100.25	100.13	99.72	100.29	100.49
Li	40	30	19	14	17	18	18	16	11	18	5	24
Rb	70	12	72	100	94	60	68	16	88	28	26	54
Ba	330	410	340	310	340	320	490	151	695	460	150	280
Sr	110	130	100	50	100	85	110	143	85	130	25	350
B	28	27		28	44	39	47	5			8.9	62
Be	1.15	0.8	4.4	1.25	1.85	1.25	1	0.9	1.25	4	0.65	1
F	1600	2400	1200	725	735	1700	1150	160	450	280	720	340
Mo	6	3.6	—	3	3.6	6.2	7	1.3	10	8	2.5	2.3
Sn	12	4.8	4	6.3	4.4	14	9.1	1.0	—	2	6.1	6.7
La	35	68	30	14	35	24	30	13	5	34	2	21
Ce	68	130	65	30	65	47	65	28	15	77	2	57
Nd	31	62	27	19	32	20	30	17	5	22	2	18
Yb	2.4	2	4.8	1.4	3.5	2.8	3	3.5	0.5	3.2	1.6	2.5
Y	23	20	34	16	36	29	30	31	15	23	11	18
Zr	110	130	100	65	90	80	90	152	60	80	40	70
Zn	770	340	400	400	140	3700	550	100	1000	200	1000	88
Pb	51	73	30	72	33	73	62	6	40	20	110	8.6
Cu	310	180	300	270	160	280	160	56	350	100	680	8.9
Cr	160	210	20	120	120	130	120	180	210	300	67	79
V	250	210	60	74	170	130	150	332	180	200	100	110
Ni	140	82	100	160	120	130	130	80	150	100	240	57
Co	43	31	60	95	37	63	46	44	70	40	130	11
Sc	19	31	—	25	25	18	23	44	34	—	9	12
Ag	1.3	0.48	—	0.34	1.35	0.86		0.07	0.15	0.1	0.83	—

Note. 1, 3, biotite–cordierite plagiogneiss (Pl, Qz, Crd, Bt, Kfs, Po, Py, and Gr); 2, biotite–cordierite plagiogneiss (Sil, Crd, Bt, Po, and Gr); 4–5, migmatized biotite–cordierite plagiogneiss (Kfs, Crd, Bt, Po, Gr, and Sil); 6, biotite–cordierite plagiogneiss (Kfs, Crd , Bt, Po, Gr, and Srp); 7, cordierite plagiogneiss (Crd, Kfs, Gr, Sil, Bt, and Po); 8–9, hypersthene plagiogneiss (Opx, Po, Bt, and Gr); 10, two-pyroxene plagiogneiss (Opx, Cpx, Bt, Po, Gr, and Chl); 11, altered two-pyroxene plagiogneiss (Opx, Cpx, Bt, Po, Gr, Chl, and Ms); 12, pyroxene–plagioclase apogneiss rock (Pl, Opx, Kfs, Bt, and Ms).
$Fe_2O_3^*$, All iron as Fe_2O_3; dash, not determined.

al., 2009), rocks of the Sharyzhalgai complex rest upon the plagiogneisses of the Onot greenstone belt, dated at 3.25–3.4 Ga (Bibikova et al., 1982, 2006).

Note that the separation of stratigraphic units in the Sharyzhalgai complex always provoked discussion (Petrova and Levitskii, 1984; Mel'nikov, 2011). This separation is partly confirmed by the data on its polychronous evolution: granulite metamorphism and transformation (granitization) (Sal'nikova et al., 2007; Levchenkov et al., 2012; Levitskiy and Levitskiy, 2014) at the Neoarchean (2.562–2.557 Ga)

and Paleoproterozoic (1.87–1.85 Ga) stages. There is also a viewpoint (Galimova et al., 2009) that the Sharyzhalgai Group (complex) is overlain by the Kitoi Group (complex), whose age varies from 2.48 to 2.53 Ga (Gladkochub et al., 2005; Levitskii et al., 2010; Glebovitskii et al., 2011).

The Cheremshanka Formation is present in the interfluve of the Kitoi and Toisuk Rivers and has no compositional analogs both among the highly metamorphosed (granulite facies) and lowly metamorphosed regional formations. The model T_{Nd}(DM) age of the metaigneous rocks (enderbites) of the Cheremshanka Formation is 3.84 Ga ($\varepsilon_{ND}(T) = -23.1$), and the protoliths of metasedimentary garnet–spinel–sillimanite–cordierite schists have T_{Nd}(DM) = 3.18 Ga ($\varepsilon_{ND}(T) = -13.2$) (Levitskii, 2012). The subsequent metamorphism of the Cheremshanka Formation is dated at 2623 ± 32 Ma (Poller et al., 2005), and the compositionally similar associations in the Kitoi complex of the Kitoi block are nearly coeval, 2.5–2.6 Ga (Levitskii et al., 2010; Glebovitskii et al., 2011). The recently obtained data on the presence of detrital zircons with ages of 3.70–2.74 Ga in high-alumina gneisses indicate the formation of their protoliths in the Mesoarchean, but their sampling point (judging by its coordinates) is located beyond the Cheremshanka Formation (Turkina et al., 2017).

Petrography and sequence of formation of the Cheremshanka Formation rocks. The study area is located in the Zhidoi block, whose southeastern part is composed predominantly of rocks probably belonging to the Zhidoi and Zoga Formations and northwestern part is formed by the rocks of the Cheremshanka Formation of the Sharyzhalgai complex (group). The Cheremshanka Formation here is composed of biotite, amphibole–biotite, garnet–biotite, and garnet–cordierite–biotite gneisses interbedded with amphibolites and with marble and calciphyre lenses and horizons. There are also horizons of amphibole–biotite, two-pyroxene, and biotite–hypersthene schists and cordierite gneisses. It is believed that the gneisses of the Cheremshanka Formation correspond to argillaceous montmorillonitic rocks and basites (Galimova et al., 2009). Primary rocks were metamorphosed under granulite facies conditions with superposed regressive metamorphism of the amphibolite facies. In addition, they underwent ultrametamorphism and migmatization related to the formation of the late Archean migmatite–granites of the Kitoi complex.

Three genetic types of rocks are recognized in the Cheremshanka Formation, which formed at the metamorphic, ultrametamorphic (magmatic), and postultrametamorphic (postmagmatic) stages (Levitskii, 2005). The share of the protoliths of orthomagmatic metamorphic rocks in the formation does not exceed 30%. In the study area they amount to no more than 2–3%. The metamorphic rocks contain minerals produced at the ultrametamorphic and postultrametamorphic stages, and the ultrametamorphic rocks have a wide range of high- and low-temperature minerals, including sulfides.

The rocks that formed at the metamorphic stage are metasedimentary biotite–cordierite (Crd, Bt, Pl, Qz; ± Opx, Po, Py, Gr), biotite (Bt, Pl, Qz; ± Crd, Sil, Po, Py, Gr), and garnet–biotite (Grt, Bt, Pl, Qz; ± Crd, Sil, Po, Py, Gr) gneisses. Orthomagmatic (pyroclastic) hyperstene (Opx, Pl, Cpx; ± Qz, Po, Py, Gr), bipyroxene (Opx, Cpx, Pl; ± Qz, Po, Py, Gr), and hypersthene–biotite (Opx, Bt, Pl; ± Qz, Po, Py, Gr) plagiogneisses and plagioschists are of limited occurrence and are reconstructed as metabasaltoids and (or) pyroclastic rocks (Petrova and Levitskii, 1984). There are also subordinate (sometimes present as thin (2–10 mm) intercalates) quartzites, quartzite–gneisses, calcitic marbles, and pyroxene calciphyres with scarce thin partings of two-pyroxene (±Bt), hypersthene (Pl, ±Gr, Opx, Crd), and cordierite-containing (±Bt, Sil, Grt, Opx) plagiogneisses and plagioschists, sometimes with graphite and sulfides (pyrrhotite, pyrite, and, extremely seldom, chalcopyrite). Both drastic and gradual transitions from cordierite- and hypersthene-containing gneisses to essentially graphite, graphite–sulfide, and sulfide–graphite rocks (pyrite ores) are observed.

The amount of sulfides in carbonate and, particularly, aluminosilicate rocks varies from few percent (single grains) to 40–50% (disseminated grains and their aggregates, veinlets, nests, and clusters (with granoblastic and lenticular segregations) conformable and unconformable with the strike of the layered strata). Sulfide segregations (intercalates, lenses, and nests) reach 15–20 cm in thickness.

Most of the polished lumps (Fig. 2) and thin sections of the samples show fine (3–5 mm) alternation of the above sulfide varieties, which indicates that these samples are metasedimentary and(or) pyroclastic. The thickness of calcitic marble and calciphyre intercalates in the gneisses varies from 2–15 cm to 2–3 m. The same stratification with the preserved unaltered protoliths of gneisses and schists is observed in the entire Cheremshanka Formation.

The rocks that formed at the ultrametamorphic stage are intensely migmatized schists and gneisses, plagioclase and K-feldspathic migmatites, and cutting granitoid bodies in gneiss and schist strata. Their amount does not exceed 10% as compared with other sites of the Sharyzhalgai uplift (e.g., 80–90% on the Baikal shore).

The rocks that formed at the postmagmatic stage are the youngest. There are both highly and weakly altered metasomatic rocks (Plyushchev et al., 1981). They are scapolitic, phlogopitic, amphibolic, zoisitic, chloritic, and also recrystallized and transformed graphite–sulfide rocks, in which pyrrhotite dominaties over pyrite and galena and chalcopyrite are also present. The rocks usually compose cutting veinlets and 0.5 mm to 5–6 cm thick nests with a sideronitic texture.

Another specific feature of the Cheremshanka Formation is the abundance of carbonate rocks (mainly calcite ones), with abundant thin (usually 1–15 cm) bodies of zonal apocarbonate and aposilicate metasomatites developed after them (Levitskii, 2005). Their rear zones are composed of periskarnic (Zharikov, 1968; Shabynin, 1973) apoaluminosilicate and(or) apocarbonate pyroxene–plagioclase and pla-

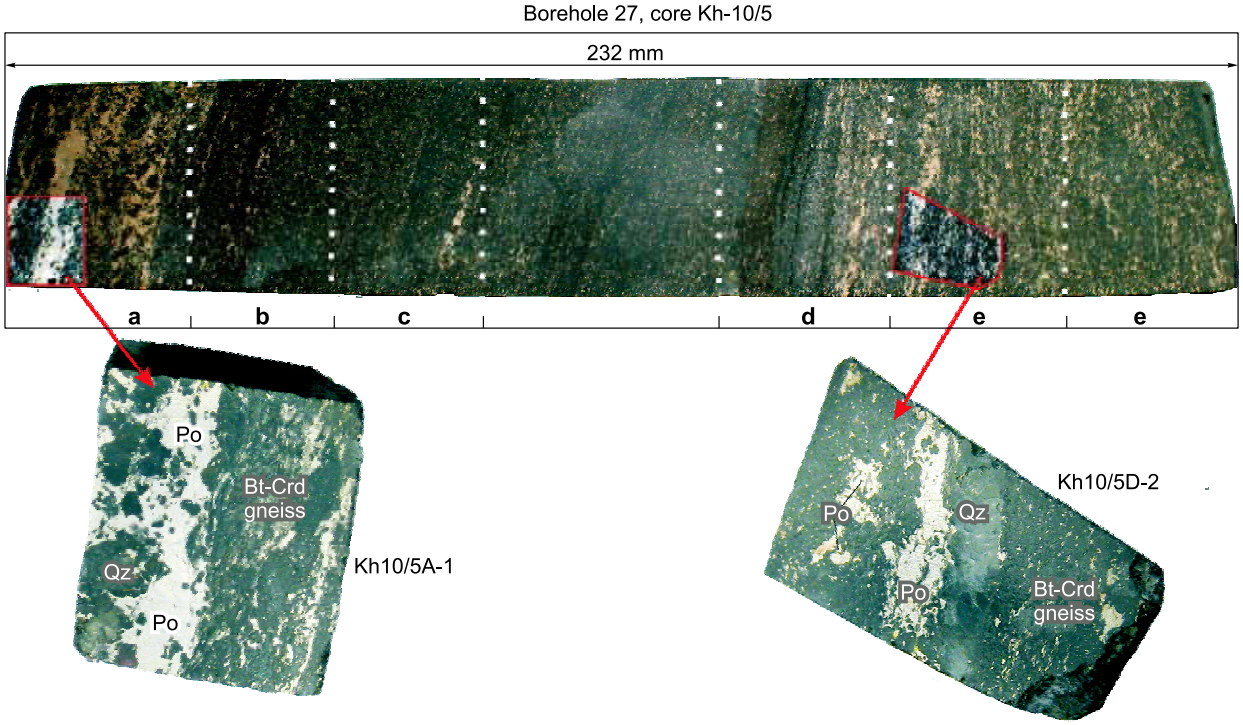

Fig. 2. Fragment of the core of borehole 27, Cheremshanka Formation (depth range 116–120 m). Veinlet-disseminated sulfide mineralization in biotite–cordierite plagiogneiss. Ore mineral segregations mark metamorphic schistosity. The sample for study was divided into several sections, which were designated by letters and numerals. Hereinafter, the minerals are designated after Whitney and Evans (2010): Act, actinolite; Ank, ankerite; Ap, apatite; Bt, biotite; Cal, calcite; Ccp, chalcopyrite; Chl, chlorite; Cpx, clinopyroxene; Crd, cordierite; Ep, epidote; Gr, graphite; Grt, garnet; Hbl, hornblende; Kfs, K-feldspar; Mgt, magnetite; Ms, muscovite; Opx, orthopyroxene; Phl, phlogopite; Pl, plagioclase; Pn, pentlandite; Po, pyrrhotite; Py, pyrite; Po, pyrrhotite; Sil, sillimanite; Spl, spinel; Srp, serpentine; Ttn, titanite; Qz, quartz.

gioclase–pyroxene rocks and apocarbonate pyroxene and apogneiss spinel–pyroxene–phlogopite metasomatites observed as conformable bodies at the contacts of schists (or gneiss) with marbles.

Petrogeochemistry of rocks. The rocks of the metamorphic stage show wide variations in contents of major and trace elements (Table 1, ans. 1, 3–7, 8, and 11). Some of them are enriched in sulfides (>4%) and graphite and can be referred to as pyrite ores. Few rock samples have abnormally high contents of Al_2O_3, Fe, MgO, CaO, P_2O_5, K_2O, S, F, Mo, Sn, and Ag, medium contents of Ba, La, Ce, Nd, Yb, Y, Pb, Cu, Cr, V, Ni, Co, and Sc, and low contents of Li, Sr Rb, and Zr (Table 1). According to the results of scintillation analysis, the rocks enriched in graphite (± pyrite and pyrrhotite) have above-clarke contents (ppm) of Au (up to 0.06), Pt (up to 0.04), and Pd (0.03).

Paleoreconstructions of metamorphic-rock compositions. By Neelov's (1980) classification, most of the protoliths of the metamorphic-stage rocks are reconstructed as argillaceous sediments: pelites; carbonate-containing and ferriferous aleuropelites; carbonate-containing mudstones; polymict, graywacke, pelite, and carbonate siltstones; and siltstone carbonate cements. Arkoses, subarkoses, and polymict, carbonate, and carbonate-ferroan sandstones are subordinate.

Calculations of geochemical modules (hydrolysate (HM), aluminosilicic (ASM), alkali (AM), titanium (TM), and normalized alkalinity (NAM) modules (Yudovich and Ketris, 2000)) showed that plagiogneisses and plagioschists with sulfide- and graphite-rich mineralization are hypohydrolysates (HM = 0.56–0.85), those with graphite-rich and sulfide-poor mineralization (HM = 0.86–2.0) are normal hydrolysates, and those with graphite- and sulfide-poor mineralization are superhydrolysates (HM = 2.1–10.0) (Table 2).

Metamorphic rocks whose protolith was pelite-silty sediments with high HM, ASM, and FM (femic module) and low AM and FFM (ferrous–ferric module) values (Table 2) are usually enriched in sulfides and graphite. Sulfide and graphite mineralization is specific to hydrolysate rocks rather than clastogene ones (grauwacke and carbonate siltstones; arkoses and subarkoses; polymict, carbonate, and carbonate-ferroan sandstones). The contents of sulfur in the rocks (Table 1) do not reach 20%, which does not permit them to be classified as sulfidolites. Note that the sulfide-richest samples (massive and densely disseminated ores) were not among the considered samples.

The share of graphite in the rocks is high; therefore, carbon-enriched gneisses and schists might be cahemoliths developed after the biogenic protolith. The measured isotopic

Table 2. HM, ASM, FM, AM, TM, IM, NAM, and FFM (Yudovich and Ketris, 2002) of plagioschists and plagiogneisses of the Cheremshanka Formation of the Sharyzhalgai complex

Rock	HM	ASM	FM	AM	TM	IM	NAM	FFM
Plagiogneisses and plagioschists with sulfide- and graphite-rich mineralization	0.89 0.49 – 1.48	0.29 0.07 – 0.38	0.68 0.24 – 1.35	0.6 0.31 – 0.97	0.07 0 – 0.22	2.48 0.01 – 10.62	0.39 0.2 – 0.64	3.36 0.97 – 7.05
Plagioschists and plagiogneisses with graphite-rich and sulfide-poor mineralization	0.69 0.67 – 0.73	0.34 0.29 – 0.37	0.43 0.40 – 0.49	0.64 0.44 – 0.9	0.11 0.06 – 0.21	0.85 0.75 – 1.06	0.32 0.25 – 0.46	7.66 5.25 – 12.27
Plagioschists and plagiogneisses with graphite- and sulfide-poor mineralization	1.47 0.41 – 7.00	0.30 0.24 – 0.37	0.47 0.21 – 0.85	1.00 0.14 – 2.72	0.08 0.03 – 0.2	1.09 0.53 – 1.72	0.29 0.13 – 0.39	7.00 1.53 – 11.71
Plagioschists and plagiogneisses with accessory or no graphite and sulfide mineralization	0.55 0.23 – 1.01	0.27 0.13 – 0.48	0.37 0.09 – 0.76	2.38 0.17 – 11.13	0.09 0.02 – 0.21	0.89 0.02 – 3.28	0.29 0.04 – 0.56	10.99 1.49 – 120.15

Note. Hydrolysate module (HM)—$(TiO_2 + AI_2O_3 + Fe_2O_3 + FeO + MnO)/SiO_2$; aluminosilicic module (AM)—Al_2O_3/SiO_2; femic module (FM)—$(Fe_2O_3 + FeO + MnO + MgO)/SiO_2$; alkali module (AM)—$Na_2O/K_2O$; titanium module (TM)—$TiO_2/ Al_2O_3$; iron module (IM) $(Fe_2O_3 + FeO + MnO)/(TiO_2 + Al_2O_3)$; normalized alkalinity module (NAM)—$(Na_2O + K_2O)/Al_2O_3$; ferrous–ferric module (FFM)—FeO/Fe_2O_3.

composition of carbon ($\delta^{13}C_{V\text{-}PDB}$) in graphite of two samples varies from –26.2 to –31.3‰, which supports the above hypothesis of the biogenic protolith. These facts indicate that the rocks containing graphite and sulfides are most likely to be metamorphosed Neoarhean–Early Paleoproterozoic analogs of black shales and the sulfides stripped by boreholes are a stratiform pyrite ore occurrence.

Sulfide mineralization. Sulfides (pyrite, pyrrhotite, and chalcopyrite) are very rare in the rocks of the Sharyzhalgai and Kitoi complexes. They are found only as accessory minerals in metaterrigenous aluminous gneisses of the granulite facies and, less often, in metaigneous apobasaltic two-pyroxene plagioschists reconstructed as normal and calc-alkalic metabasalts and in apocarbonate and apoaluminosilicate metasomatites formed at the ultrametamorphic and postultrametamorphic stages.

Pyrrhotite, pyrite, and chalcopyrite are widespread in paragenesis with graphite in the Cheremshanka Formation. They are present as small conformable segregations and uniform dissemination in paragneisses, orthogneisses, and orthoschists of the granulite facies formed at the metamorphic stage. In superposed rocks formed at the ultrametamorphic and postultrametamorphic stages, high-temperature parageneses are replaced by low-temperature ones and all minerals, including graphite and sulfides, are recrystallized and occur as unevenly distributed segregations of different sizes and veins cutting metamorphic schistosity.

A typical example of sulfide ores formed at the metamorphic stage and subjected to partial transformations is the sample Kh10/5 (Fig 2, borehole 27). Its sulfide ore is composed mostly of pyrrhotite with relict pyrite and, to a lesser extent, chalcopyrite and sphalerite grains. Figure 3 shows a small fragment of the core (Fig. 2, Kh10/5D-2), where biotite–cordierite plagiogneiss contains vein, nest-disseminated, and finely disseminated sulfide mineralization. Veinlet–nest mineralization prevails in the top of the sample (Fig. 3*A*), and finely disseminated one, in the bottom. In the middle of the sample, there is a quartz veinlet almost free of sulfides, located parallel to a small sulfide vein.

The structure of the sulfide veinlet in which the isotopic composition of sulfur was studied is shown in Fig. 3*B*, *C*, *D*. The veinlet is composed mostly of pyrrhotite with preserved pyrite relics. Pyrite makes contact with pyrrhotite via a thin magnetite reaction rim.

The rock hosting sulfide mineralization is composed of cordierite, isometric biotite grains, and elongate graphite crystals. There is a magnetite–ankerite reaction rim at the boundary of the ore veinlet and the host silicates (Fig. 3*C*). The magnetite rim contains finest pyrite grains. Pyrrhotite of the veinlet contains irregular-shaped chalcopyrite inclusions (Ccp_1, Fig. 3*C*), trapped graphite crystals, and irregular-shaped pyrite fragments with a magnetite rim. The pyrite contains fine chalcopyrite segregations (Ccp_2, Fig. 3*C*) differing in composition from the chalcopyrite in the pyrrhotite.

Figure 3*D* shows the mineral relationship at the lower boundary of the ore veinlet. There is also a magnetite–ankerite reaction rim. Graphite, cordierite, and biotite form complex intergrowths at the site between the quartz and ore veinlets. We examined this site by elemental mapping (Fig. 3, elemental mapping, *D*). Sulfide rocks (ores) are localized mostly in the upper part of the map and are well detected from a high content of sulfur. A fragment of a quartz veinlet is visible by the high intensity of silicon (white). Cordierite (light gray) and biotite (dark gray) are well identified from the Al X-ray spectrum, and biotite is easily distinguished on the Mg X-ray map. The Ca X-ray spectra show the presence of ankerite. The Fe X-ray map reveals magnetite rims and grains (white), sulfides (light gray) (pyrite and pyrrhotite are not distinguished here), and biotite (dark gray).

All this testifies to the intricate multistage evolution of sulfides in the rocks and ores of the Cheremshanka Forma-

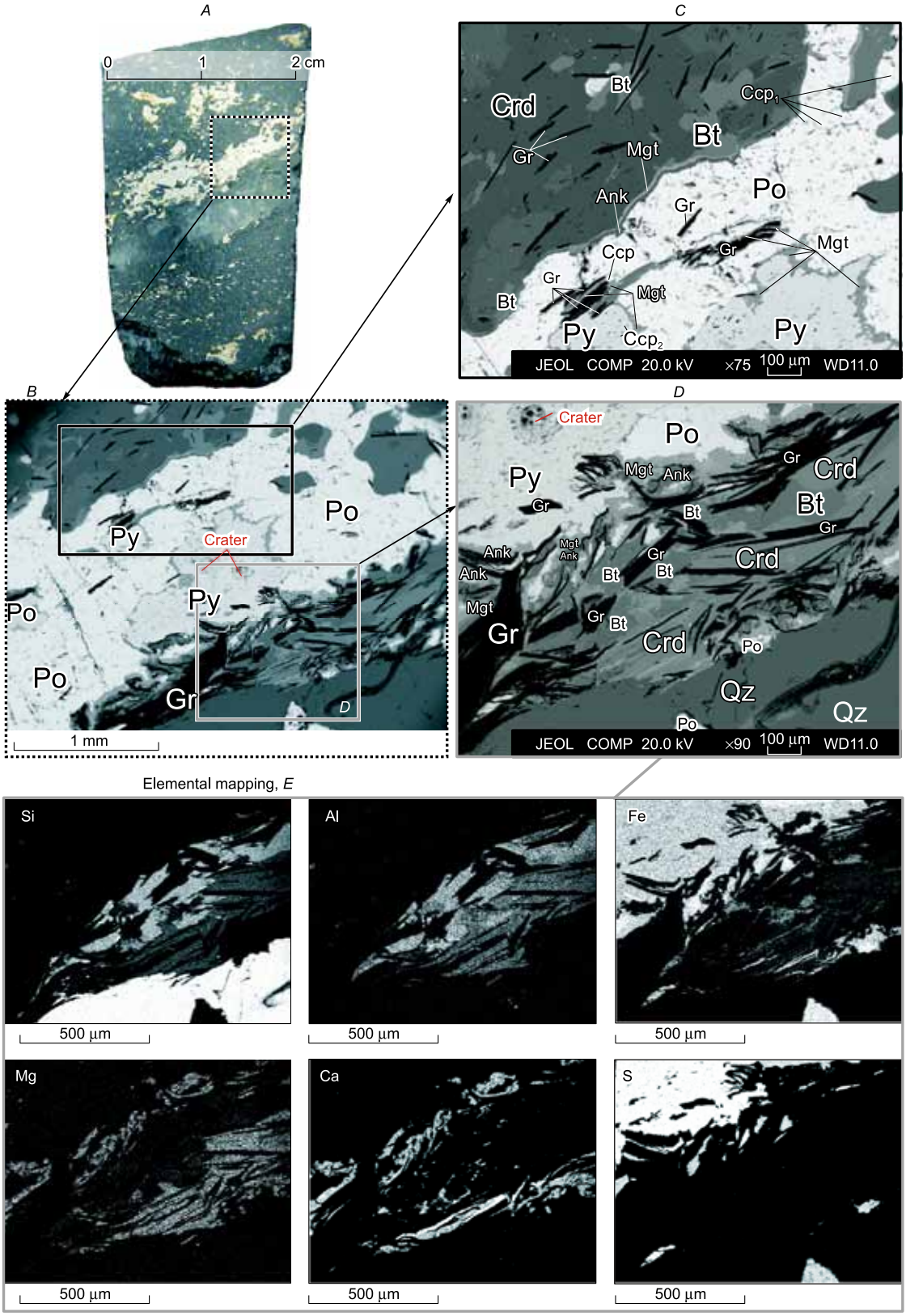

Fig. 3. Structure and mineral compositions of the sulfide ore sample Kh10/5D-2 from the core of borehole 27. Veinlet-disseminated mineralization (fragment *A*) in biotite–cordierite plagiogneiss is predominantly pyrrhotite. Pyrite relics with fine chalcopyrite grains (fragment *B*) in pyrrhotite have a magnetite reaction rim (fragment *C*). At the boundary with the host silicates, pyrrhotite periodically has a rim of alternating magnetite and ankerite. The silicate matrix bordering the vein contains biotite, cordierite, and graphite (fragments *C* and *D*). Although most of graphite is localized mainly in the silicate matrix, there are few fine graphite segregations in the pyrrhotite. The minerals are oriented in the same direction as metamorphogene schistosity. Elemental mapping of the fragment *D* shows the relationship among the minerals in detail.

Table 3. Characteristics of the samples and their contents of sulfur isotopes (‰)

No.	Bore-hole	Subsurface depth, m	Sample	Type of rock and mineral assemblage	Analyzed mineral	$\delta^{33}S$	$\delta^{34}S$	$\Delta^{33}S$
1	BH-7	30–32	Kh1/9	Pyroxene–plagioclase rock with disseminated sulfide mineralization (apocarbonate rock formed at the ultrametamorphic stage; Pl, Cpx, Cal, Gr, Bt, Ep, Po, and Chl)	Pyrrhotite	3.50	3.66	1.61
					Pyrrhotite	3.47	3.77	1.52
2		36	Kh1/12	Alternating quartzites and garnet–biotite quartzite–gneisses with weak sulfide dissemination (Qz, Gr, Bt, and Po)	Pyrrhotite	4.12	3.73	2.20
					Pyrrhotite	4.10	3.97	2.06
					Pyrrhotite	4.10	4.02	2.03
3		38	Kh1/15	Biotite–cordierite plagiogneiss (Pl, Qz, Crd, Bt, Kfs, Po, Py, and Gr)	Pyrite	4.29	4.90	1.76
					Pyrrhotite	3.60	3.59	1.75
4		42	Kh1/16	Biotite–cordierite plagiogneiss with sillimanite (Pl, Qz, Sil, Crd, Bi, Po, Py, and Gr)	Pyrite	4.47	3.89	2.41
					Pyrrhotite	3.71	2.42	2.46
5		59	Kh1/28	Hypersthene gneiss with sulfide dissemination (Opx, Pl, Qz, Cpx, Bt, Po, and Gr)	Pyrrhotite	5.40	5.35	2.65
					Pyrrhotite	5.31	5.13	2.66
					Pyrrhotite	5.15	4.91	2.62
					Pyrrhotite	4.72	4.09	2.64
6		79	Kh1/31b	Hypersthene plagiogneiss with poor sulfide dissemination (Cpx, Pl, Qz, Bt, Po, and Gr)	Pyrrhotite	3.14	3.69	1.24
					Pyrrhotite	3.17	3.79	1.22
					Pyrrhotite	2.98	3.40	1.23
7		157	Kh1/35	Two-pyroxene plagiogneiss with weak sulfide dissemination (Cpx, Opx, Pl, Qz, Bt, Po, Gr, and Chl)	Pyrrhotite	1.53	1.97	0.51
8		162	90–181	Pyroxene (hedenbergite) skarn with sulfides (Cpx, Bt, Pl, Hbl, Act, Cal, Py, Po, and Ccp)	Chalcopyrite	3.30	2.50	2.00
					Pyrrhotite	3.30	2.60	1.99
					Pyrrhotite	3.20	2.40	1.95
9		177	Kh1/37	Cordierite plagiogneiss with weak sulfide dissemination (Pl, Oz, Crd, Bt, Kfs, Po, Py, and Gr)	Pyrite	5.12	4.80	2.64
					Pyrrhotite	4.69	3.85	2.70
10		177.5	Kh1/38b	Biotite–cordierite plagiogneiss (Pl, Qz, Kfs, Crd, Sil, Bt, Po, and Gr)	Pyrrhotite	4.99	4.49	2.67
11		178.5	90–183	Sulfide rocks (low-grade ores) in fine-grained gneisses (Po, Py, Gr, Pl, Qz, Kfs, and Crd)	Pyrrhotite	2.3	3.3	0.58
					Pyrite	3.0	4.7	0.57
					Pyrrhotite	2.5	3.5	0.66
12		179.3	Kh1/40	Graphite–pyrrhotite–cordierite plagiogneiss with disseminated sulfide mineralization (Pl, Qz, Kfs, Sil, Crd, Bt, Po, and Gr)	Pyrite	5.56	5.55	2.70
					Pyrrhotite	4.79	4.11	2.66
13	BH-11	167	Kh11/3	Two-pyroxene plagiogneiss with disseminated sulfide mineralization (Pl, Qz, Cpx, Opx, Bt, Hbl, Gr, Po, and Py)	Pyrite	6.07	5.00	3.49
					Pyrrhotite	5.21	3.29	3.50
					Pyrrhotite	4.54	2.13	3.43
					Pyrrhotite	4.78	2.58	3.44
					Pyrrhotite	4.63	2.18	3.49
					Pyrrhotite	4.55	2.05	3.49
14		205	Kh11/7a	Altered two-pyroxene plagiogneiss with weak sulfide dissemination (Pl, Qz, Opx, Cpx, Bt, Po, Gr, Chl, and Ms)	Pyrrhotite	2.85	2.49	1.56
					Pyrrhotite	2.33	1.73	1.44
					Pyrrhotite	2.34	1.82	1.40
15	BH-12	87.3–95.6	Kh6/1	Pyroxene calciphyre (apocarbonate rock formed at the ultrametamorphic stage; Cpx, Qz, Pl, Kfs, Gr, and Py)	Pyrite	3.55	4.87	1.05
					Pyrite	3.59	4.95	1.05
16		308.5	90–88	Pyrrhotite rocks (massive ores) in biotite–cordierite plagiogneiss (Po)	Pyrrhotite	0.32	3.55	–1.40
					Pyrrhotite	0.37	3.41	–1.39
					Pyrrhotite	0.13	3.21	–1.52
					Pyrrhotite	0.22	3.27	–1.46
					Pyrrhotite	0.14	1.18	–1.49
					Pyrrhotite	0.06	2.94	–1.45

(*continued on next page*)

Table 3 (*continued*)

No.	Borehole	Subsurface depth, m	Sample	Type of rock and mineral assemblage	Analyzed mineral	$\delta^{33}S$	$\delta^{34}S$	$\Delta^{33}S$
17	BH-12	312.5	90–90_1	Monomineral pyrrhotite rocks (massive ores) in biotite–cordierite plagiogneiss (Po and Ccp)	Pyrrhotite	3.18	3.93	1.15
					Pyrrhotite	3.16	3.88	1.16
					Chalcopyrite	3.12	3.75	1.20
18		313.6	90–91	Monomineral pyrrhotite rocks (nest ores) in biotite–cordierite plagiogneiss (Po)	Pyrrhotite	3.40	4.56	1.05
					Pyrrhotite	3.32	4.33	1.09
19		314	90–92	Monomineral pyrrhotite rocks (nest ores) in biotite–cordierite plagiogneiss (Po)	Pyrrhotite	3.47	3.82	1.50
					Pyrrhotite	3.47	3.84	1.49
20		505	Kh14a	Pyroxene calciphyre (apocarbonate rock formed at the ultrametamorphic stage, with pyrrhotite dissemination; Cal, Cpx, Hbl, Act, Ttn, Qz, Gr, and Po)	Pyrrhotite	1.82	2.81	0.37
					Pyrrhotite	1.82	2.91	0.32
21		505	Kh14b	Highly amphibolized plagioclase–pyroxene rock with scarce pyrrhotite (apocarbonate rock formed at the ultrametamorphic stage; Cpx, Hbl, Act, Pl, Kfs, Qz, Ttn, and Po)	Pyrrhotite			
						0.24	0.76	–0.15
22	BH-13	52	Kh5/2a	Pyroxene–plagioclase rock (apogneissic rock formed at the ultrametamorphic stage; Pl, Opx, Kfs, Bt, Ms, Po, and Gr)	Pyrrhotite	1.55	1.55	0.75
					Pyrrhotite	1.29	1.19	0.67
23	BH-27	**51**	Kh10/2	Spinel–pyroxene–phlogopite rock with sulfides and pyrrhotite (apogneissic rock with relict minerals, formed at the ultrametamorphic (Opx, Spl, Pl, Po, Gr, and Ap) and postultrametamorphic (Phl, Chl, and Ms) stages)	Pyrrhotite	4.07	5.52	1.22
					Pyrrhotite	4.10	5.52	1.26
					Pyrrhotite	3.86	5.50	1.02
24		108–112	Kh10/4	Biotite–cordiderite plagiogneiss with pyrrhotite dissemination (Pl, Qz, Kfs, Crd, Bt, Po, Gr, and Srp)	Pyrrhotite	5.02	4.66	2.62
					Pyrrhotite	4.85	4.25	2.65
25		116–120	Kh10/5v	Altered and highly migmatized biotite–cordierite plagiogneiss with myrmekites, weak pyrrhotite dissemination, and superposed biotitization (Pl, Qz, Kfs, Crd, Bt, Po, and Gr)	Pyrrhotite	3.24	6.29	0.002
					Pyrrhotite	2.82	5.45	0.014
					Pyrrhotite	2.65	5.21	-0.029
					Pyrrhotite	2.74	5.31	0.01
26		116–120	Kh10/5A–1	Veinlet-disseminated sulfide rocks (ores) in biotite–cordierite plagiogneiss (Pl, Bt, Crd, Kfs, Po, and Gr)	Pyrrhotite	4.10	3.29	2.41
					Pyrrhotite	3.73	2.56	2.41
			Kh10/5B–3	Biotite–cordierite plagiogneiss with disseminated fine sulfide grains (Pl, Qz, Bt, Crd, Kfs, Po, and Gr)	Pyrrhotite	3.97	2.87	2.49
					Pyrrhotite	3.91	2.77	2.49
			Kh10/5C–2	Biotite–cordierite plagiogneiss with disseminated fine sulfide grains (Pl, Qz, Bt, Crd, Po, and Gr)	Pyrrhotite	4.02	2.71	2.62
			Kh10/5D–1	Biotite–cordierite plagiogneiss with disseminated fine sulfide grains (Pl, Qz, Bt, Crd, Kfs, Py, and Gr)	Pyrite	4.43	3.39	2.68
					Pyrite	4.16	3.11	2.56
			Kh10/5E–2	Biotite–cordierite plagiogneiss with disseminated fine sulfide grains (Pl, Qz, Bt, Crd, Kfs, Py, and Gr)	Pyrite	4.16	3.37	2.42
					Pyrite	4.09	3.14	2.48
				Veinlet-disseminated sulfide rocks (ores) in biotite–cordierite plagiogneiss (Py, Pl, Bt, Crd, Kfs).	Pyrite	4.08	3.46	2.30
					Pyrite	4.07	3.31	2.37
					Pyrite	4.09	3.31	2.39
			Kh10/5G–3		Pyrite	4.16	3.40	2.41
27		120–124	Kh10/6	Migmatized biotite–cordierite plagiogneiss with graphite and evenly distributed disseminated fine sulfide grains (Pl, Qz, Po, Crd, Kfs, Gr, Sil, and Bt)	Pyrrhotite	5.56	5.58	2.69
					Pyrrhotite	5.51	5.41	2.73
					Pyrrhotite	5.19	5.27	2.48
					Pyrrhotite	5.43	5.20	2.75
					Pyrrhotite	5.16	5.10	2.53
					Pyrrhotite	4.97	4.25	2.64
					Pyrrhotite	4.90	4.33	2.67

Note. Ap, Apatite; Act, actinolite; Bt, biotite; Cal, calcite; Ccp, chalcopyrite; Qz, quartz; Gr, graphite; Grt, garnet; Kfs, K-feldspar; Crd, cordierite; Hbl, hornblende; Cpx, clinopyroxene; Ms, muscovite; Pl, plagioclase; Opx, orthopyroxene; Py, pyrite; Po, pyrrhotite; Sil, sillimanite; Ttn, titanite; Phl, phlogopite; Spl, spinel; Spn, serpentinte; Chl, chlorite.

tion, from the origin of their protoliths to the transformations at the subsequent stages.

Geochemistry of sulfur isotopes in the rocks of the Cheremshanka Formation. Sulfide minerals of the Cheremshanka Formation rocks are characterized by a narrow range of $\delta^{34}S$ values (from 0.76 to 6.3‰); most of these values fall in the range $2.5 < \delta^{34}S < 5.5$‰ (Table 3). The minimum value of $\delta^{34}S$ has been established for pyrrhotite from amphibolized apocarbonate plagioclase–pyroxene rock (obviously allochemical) formed at the ultrametamorphic stage (Table 3, sample 19 (Kh14b)), and the maximum value, for pyrrhotite from biotite–cordierite plagiogneiss formed at the metamorphic stage (Table 3, sample 26 (Kh10/5)). The values $\delta^{34}S \approx 0$‰ are usually interpreted as mantle ones, and positive values of $\delta^{34}S$ are explained by the involvement of sulfur of sedimentary sulfates in the ore process (Grinenko and Grinenko, 1974). For pyrite ores, such values are related to the mixing of sulfur leached during the dissolution of magmatic sulfides ($\delta^{34}S \approx 0$‰) of oceanic crustal rocks and the reduction of seawater sulfates ($\delta^{34}S \approx 21$‰) (Grichuk and Lein, 1991). In general, sulfide ores of hydrothermal systems of recent oceans are characterized by a narrow range of $\delta^{34}S$ values, $0 < \delta^{34}S < 6$ ‰ (Butler et al., 1998). The obtained $\delta^{34}S$ values of sulfides of the Cheremshanka Formation rocks fit this range.

The $\delta^{33}S$ values also vary over a narrow range, $0.24 < \delta^{33}S < 6.07$‰, but only part of them is in accord with mass-dependent fractionation. Most of the studied sulfide samples from the Cheremshanka Formation carry MIF-S signals (Table 3). Their $\Delta^{33}S$ values vary from –1.44 to +3.49‰.

Significant MIF-S anomalies (2.4 to 3.5‰) are associated with rocks formed at the metamorphic stage: two-pyroxene plagiogneisses, cordierite gneisses, quartzite–gneisses, and quartzites (Table 3). The rocks that underwent ultrametamorphism and metasomatism are characterized by lower $\Delta^{33}S$ values ($1.5 < \Delta^{33}S < 0.5$‰). The youngest metasomatic rocks show negligible $\Delta^{33}S$ values, not exceeding ±0.5‰.

The mineral relationships show that most of pyrrhotite replaced **pyrite** during granulite metamorphism, although part of it might be of primary origin. A specific feature of the Cheremshanka Formation sulfides is the heavier sulfur isotope composition ($\delta^{34}S$ and $\delta^{33}S$) in pyrites as compared with pyrrhotite, while the $\Delta^{33}S$ anomaly remains nearly the same. The $\delta^{34}S$ values in pyrite are 0.95–2.80‰ higher than those in pyrrhotite. Under isotope equilibrium, such a partitioning of sulfur corresponds to the temperature range 50–320 ºC (Kajiwra and Krouse, 1971). These temperatures are much lower than the temperature calculated with mineral geothermometers for the host rocks that underwent metamorphism of the granulite facies. This indicates that either an isotope equilibrium in sulfides was established at the final (regressive) stages of ultrametamorphic and postultrametamorphic transformations or pyrrhotite and pyrites are nonequilibrium (heterogeneous and heterochronous).

DISCUSSION

The present-day Cheremshanka Formation is made up of rock complexes resulted from the high-pressure high-temperature transformation of their protolith. Their primary appearance completely changed and can be reconstructed only with the use of special techniques (Predovskii, 1970; Neelov, 1980; Yudovich and Ketris, 2000). According to the results of a chemical analysis of the rocks, they were initially hydrolysates. Most of them are reconstructed as sedimentary rocks, mainly clays, including arkoses and subarkoses, and as polymict, carbonate, and carbonate-ferriferrous sandstones, i.e., rocks of underwater origin. Sulfides are present in them as fine segregations, unevenly distributed dissemination, and intercalates of massive ores. All this indicates that the studied rocks are, most likely, metamorphosed Neoarchean–Early Paleoproterozoic analogs of black shales and the sulfides stripped by boreholes are stratiform pyrite ores.

Sulfur in stratiform pyrite deposits can be of three genetic types: magmatic sulfur, sedimentary atmospheric sulfur, and seawater sulfate sulfur. There is a viewpoint that magmatic sulfur is predominant in such deposits (Huston et al., 2001). However, studies of recent hydrothermal seafloor systems, which are considered to be equivalents of ancient pyrite deposits, showed that seawater sulfate makes a great contribution to the total content of sulfur in ores, up to 40% or even more (Ono et al., 2007; Peters et al., 2010; Farquhar et al., 2010, 2013). A recent study of Australian deposits has shown that the contribution of seawater sulfate to the total content of sulfur in stratiform pyrite deposits is 2 to 30%, which is close to that in recent hydrothermal deposits (Jamieson et al., 2013; Chen et al., 2015). But the $\delta^{34}S$ values alone are not sufficient for estimating the contribution of sedimentary sulfur, especially that from the ancient Archean atmosphere. We tried to determine the sources of sulfur involved in the formation of sulfides of the Cheremshanka Formation, based on the multiple sulfur isotope composition.

According to laboratory experiments and atmospheric-chemistry models, MIF-S results from photochemical reactions of sulfur-bearing species in the anoxic early Earth's atmosphere (Farquhar et al., 2000; Pavlov and Kasting, 2002). Sulfur dioxide (SO_2) released into the atmosphere during volcanic activity has mantle $\delta^{34}S$ and $\delta^{33}S$ values and $\Delta^{33}S \sim 0.0$. Photochemical dissociation of volcanogenic SO_2 in the anoxic atmosphere can result in elemental sulfur (S_8) with positive $\delta^{34}S$ and $\Delta^{33}S$ values and sulfate with negative $\delta^{34}S$ and $\Delta^{33}S$ values (Ono et al., 2003; Farquhar et al., 2014). Most of the $\Delta^{33}S$ values in Archean sulfide minerals are the result of mixing (in different proportions) of photolytic elemental sulfur and sulfate (Wacey et al., 2010; Roerdink et al., 2012; Wacey et al., 2015).

Most of the sulfides in the Cheremshanka Formation have positive $\delta^{34}S$ and $\Delta^{33}S$ values, i.e., photolytic elemental sulfur might have been the source of isotopic anomaly reported here. Most of the points in the $\delta^{34}S$–$\Delta^{33}S$ diagram lie

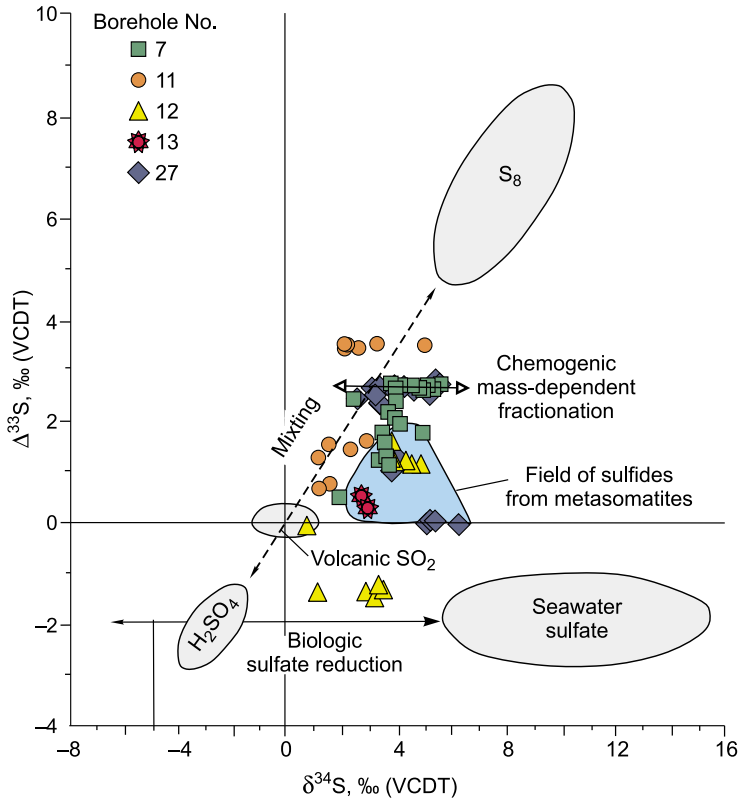

Fig. 4. Correlation between sulfur isotopes in sulfides from the Cheremshanka Formation rocks. Atmospheric mass-independent fractionation is shown by a dashed arrow. The direction of mass-dependent fractionation under recrystallization during metamorphism is shown by a double-ended arrow. Gray fields mark the isotope composition of volcanic SO_2, S_8, and H_2SO_4 aerosols and seawater sulfate (Ono et al., 2003). Blue field corresponds to sulfides of the Cheremshanka Formation metasomatites.

in the field of isotope mixing of volcanic sulfur and atmospheric sulfur (Fig. 4).

Besides elemental sulfur, sulfate sulfur was also involved in the formation of the Cheremshanka Formation sulfides. However, sulfides with negative $\Delta^{33}S$ values are extremely rare among the studied rocks. This might be due to both the incomplete sampling of rocks and the specific formation of the unit. For example, the results of our preliminary studies (Vysotskii et al., 2016) showed mostly negative $\Delta^{33}S$ values of sulfides in the Onot and Kitoi complexes of the Sharyzhalgai uplift of the Siberian craton basement. If the next investigations confirm this differentiation, then it can be used for the structural and chemical correlations of the regional metamorphic units.

There is no doubt that the primary atmospheric MIF-S signal can be modified during geologic processes. However, sulfur with an MIF-S anomaly might have got to the sediment only at the moment of its formation, whereas volcanic sulfur might have been introduced at any time throughout the geologic history of the rocks under study, including the periods of their metamorphism and metasomatism.

Multiple sulfur isotope signatures in the rocks of the Cheremshanka Formation mark two processes: biologic (bacterial) sulfate reduction and metamorphic recrystallization.

Bacterial sulfate reduction, related to bacteria activity, might already have existed 3.4 billion years ago (Ohmoto et al., 1993; Shen et al., 2001). Biologic sulfate reduction and subsequent formation of pyrite in sedimentary rocks might have been the main mechanism of absorption of seawater sulfate at the Late Archean–Early Paleoproterozoic boundary. Biologic sulfate reduction leads to a $\delta^{34}S$ increase in the product up to ~50‰ relative to the primary sulfate (Ohmoto and Goldhaber, 1997; Canfield, 2001). Sulfides resulted from the biologic reduction of photolytic sulfate have a lighter isotopic composition of sulfur, and the residual sulfate has a heavier one (Fig. 4).

We recorded traces of this process in one of the samples from borehole 12 (Fig. 4). Its sulfides are poor in light sulfur isotope (the minimum $\delta^{33}S$ value) but show a high negative $\Delta^{33}S$ value. Their figurative points are arranged along the line connecting the fields of seawater sulfates and photolytic sulfate. The distribution of sulfur isotopes in the studied pyrrhotites is uneven, which might be due to both primary inhomogeneities and subsequent metamorphic recrystallization.

Metamorphogene recrystallization. Sulfides of the Cheremshanka Formation are divided into several groups with close $\delta^{34}S$ but different $\delta^{33}S$ values. A few figurative points of the sulfides are arranged along the MDF trend

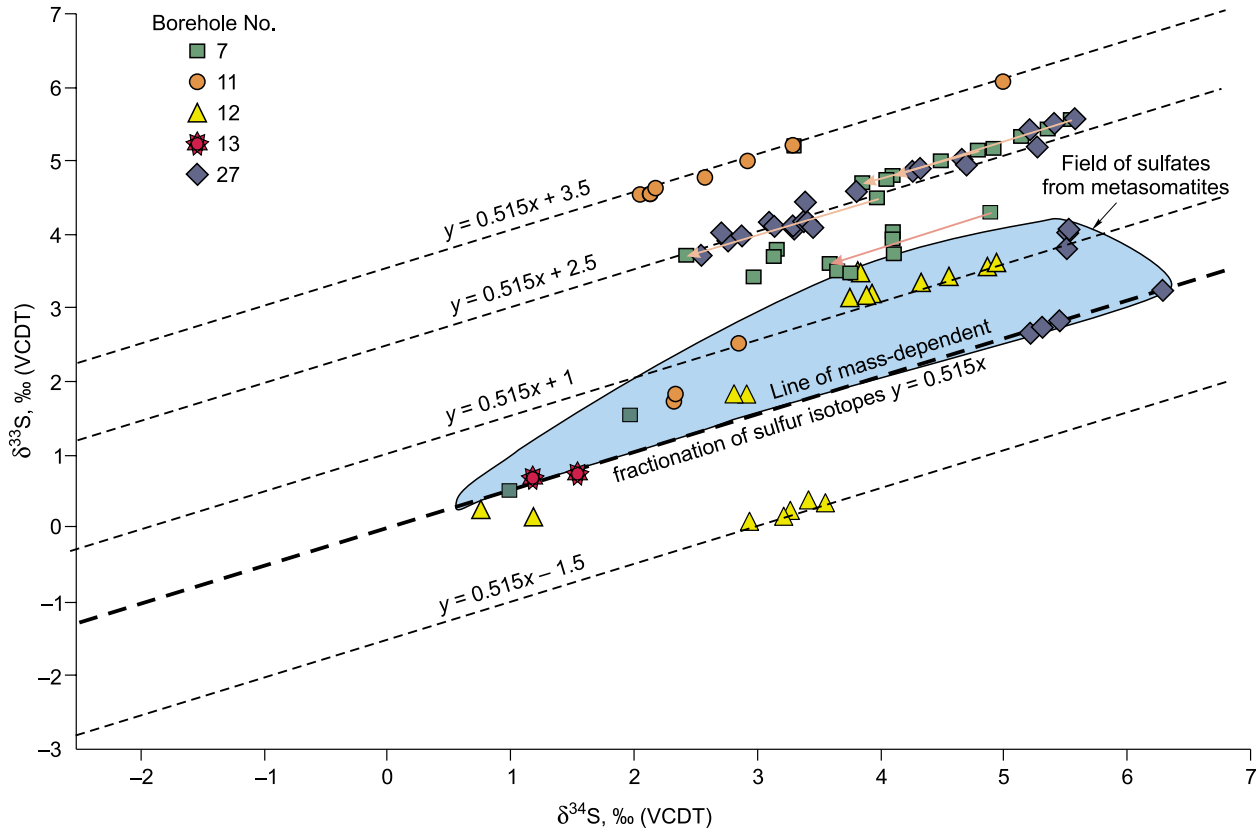

Fig. 5. $\delta^{34}S$–$\delta^{33}S$ diagram for sulfides from the Cheremshanka Formation rocks. Arrows connect pyrrhotite and pyrite from the same sample. Blue field corresponds to sulfides of the Cheremshanka Formation metasomatites.

(Fig. 5). These are sulfides disseminated in skarns and metasomatites. Probably, part of their sulfur was supplied with a magmatogene fluid during later ultrametamorphic and postultrametamorphic transformations. This sulfur had mantle parameters. Mixing of sulfur from different sources disturbed the primary isotope ratios; as a result, the $\Delta^{33}S$ signature was strongly diluted or even vanished.

Most sulfides of rocks of different compositions and genesis preserve the $\Delta^{33}S$ signature, forming a series of lines subparallel to the MDF trend. These trends reflect two factors: (1) the average $\Delta^{33}S$ value for the sulfides of this group, i.e., the average relative amount of sulfur that has passed through atmospheric transformations, and (2) the scale of sulfur fractionation during subsequent superposed processes.

After the formation of the $\Delta^{33}S$ signature, during isochemical granulite metamorphism, mass-dependent fractionation of sulfur isotopes took place, but the $\Delta^{33}S$ value remained constant. This is evidenced by the sulfur isotope composition trends ($\delta^{34}S$, $\delta^{33}S$, and $\Delta^{33}S$) of coexisting early pyrites and superposed late pyrrhotites (Table 3, Figs. 4 and 5). It is seen that the maximum amount of sedimentary sulfur ($2.5 < \Delta^{33}S < 3.5$‰) is present in sulfides of rocks formed at the metamorphic stage, which were slightly subjected to subsequent ultrametamorphism (granitization) and metasomatism.

Granitization and metasomatism were accompanied by the inflow of sulfur with other (mantle?) parameters. This sulfur had the maximum amount of the heavy isotope ($\delta^{34}S$ = 5.0–6.3‰) and no MIF-S anomaly. Pyrrhotite with such isotopic parameters is present in biotite migmatite developed after cordierite plagiogneiss (sample Kh10/5V).

The less the rocks are metasomatized, the less was the inflow of additional sulfur, the less was the dilution of $\Delta^{33}S$, and the higher was its residual value. At the same time, recrystallization caused by high-gradient isochemical metamorphism changed the $\delta^{34}S$ and $\delta^{33}S$ values but did not change the $\Delta^{33}S$ value. As a result, the $\delta^{34}S$ and $\delta^{33}S$ lines are subparallel to the main trend of mass-dependent sulfur fractionation and are spaced the value of $\Delta^{33}S$ from it.

CONCLUSIONS

The above data on the petrogeochemical composition of the studied objects show that most of the rocks of the Cheremshanka Formation are metamorphosed Late Archean hydrolysates, compositional analogs of black shales. The sulfide mineralization of the Cheremshanka Formation is of stratiform pyrite type.

The multiple sulfur isotope composition in the sulfides of the Cheremshanka Formation unambiguously indicates the presence of sedimentary sulfur that has passed through atmospheric transformations. Despite the high-grade metamorphism and the subsequent ultrametamorphic (granitization) and post ultrametametamorphic transformations accompanied by a change in the primary mineral composition of rocks and by chemogenic fractionation of sulfur, the signature of the atmospheric source of sulfur in sulfide ores has been well preserved. In rocks subjected to metasomatism, the signature of sedimentary sulfur was diluted by supplied sulfur with mantle parameters or even vanished.

The section of the Cheremshanka Formation of the Sharyzhalgai Group is an example of stratification of exogenous rocks formed at the Archean–Proterozoic boundary. The obtained results on sulfur isotopy can be invoked for substantiation of the Precambrian structural and petrogeochemical scale of this and other regions and for correlation of their rocks with other Precambrian complexes.

This work was supported by grants 15-05-00740 and 17-05-00469 from the Russian Foundation for Basic Research.

REFERENCES

Bekker, A., Holland, H.D., Wang, P-L., Rumble, D. III, Stein, H.J., Hannah, J.L., Coetzee, L.L, Beukes, N.J., 2004. Dating the rise of atmospheric oxygen. Nature 427 (6970), 117–120.

Bibikova, E.V., Khil'tova, V.Ya., Gracheva, T.V., Makarov, V.A., 1982. The age of greenstone belts of the Sayan area. Dokl. Akad. Nauk SSSR 267 (5), 1171–1174.

Bibikova, E.V., Turkina, O.M., Kirnozova, T.I., Fukzan, M.M., 2006. Ancient plagiogneisses of the Onot block of the Sharyzhalgai metamorphic massif: isotopic geochronology. Geochem. Int. 44 (3), 310–315.

Butler, I.B., Fallick, A.E., Nesbitt, R.W., 1998. Mineralogy, sulphur isotope geochemistry and the development of sulphide structures at the Broken Spur hydrothermal vent site, 29010'N, Mid-Atlantic Ridge. J. Geol. Soc. 155, 773–785.

Canfield, D.E., 2001. Biogeochemistry of sulfur isotopes. Rev. Miner. Geochem. 43 (1), 607–636.

Chen, M., Campbell, I.H., Xue, Y., Tian, W., Ireland, T.R., Holden, P., Cas, R.A.F., Hayman, P.C., Das, R., 2015. Multiple sulfur isotope analyses support a magmatic model for the volcanogenic massive sulfide deposits of the Teutonic Bore Volcanic Complex, Yilgarn Craton, Western Australia. Econ. Geol. 110, 1411–1423.

Farquhar, J., Wing, B., 2003. Multiple sulfur isotopes and the evolution of the atmosphere. Earth Planet. Sci. Lett. 213 (1–2), 1–13.

Farquhar, J., Bao, H., Thiemens, M.H., 2000. Atmospheric influence of Earth's earliest sulfur cycle. Science 289, 756–759.

Farquhar, J., Wu, N.P., Canfield, D.E., Oduro, H., 2010. Connections between sulfur cycle evolution, sulfur isotopes, sediments, and base metal sulfide deposits. Econ. Geol. 105 (3), 509–533.

Farquhar, J., Cliff, J., Zerkle, A.L., Kamyshny, A., Poulton, S.W., Claire, M., Adams, D., Harms, B., 2013. Pathways for Neoarchean pyrite formation constrained by mass-independent sulfur isotopes. Proc. Nat. Acad. Sci. U.S.A. 110 (44), 17,638–17,643.

Farquhar, J., Zerkle, A.L., Bekker, A., 2014. Geologic and geochemical constraints on Earth's early atmosphere, in: Holland, H.D., Turekian, K.K. (Eds.), Treatise on Geochemistry. Elsevier, Amsterdam, Vol. 6, pp. 91–138.

Galimova, T.F., Permyakov, S.A., Bobrovskii, V.T., Pashkova, A.G., Bormotkina, L.A., Povarintseva, S.A., Matveichuk, A.A., Namolova, M.M., Sadriev, V.M., 2009. State Geological Map of the Russian Federation, Scale 1:1,000,000 [in Russian]. Kartograficheskaya Fabrika VSEGEI, St. Petersburg.

Gladkochub, D.P., Donskaya, T.V., Mazukabzov, A.M., Sal'nikova, E.B., Sklyarov, E.V., Yakovleva, S.Z., 2005. The age and geodynamic interpretation of the Kitoi granitoid complex (southern Siberian craton). Russian Geology and Geophysics (Geologiya i Geofizika) 46 (11), 1121–1133 (1139–1150).

Glebovitskii, V.A., Levchenkov, O.A., Levitskii, V.I., Rizvanova, N.G., Levskii, L.K., Bogomolov, E.S., Levitskii, I.V., 2011. Age stages of metamorphism at the Kitoi sillimanite schist deposit, southeastern Prisayan'e. Dokl. Earth Sci. 436 (1), 13–17.

Golding, S.D., Duck, L.J., Young, E., Baublys, K.A., Glikson, M., Kamber, B.S., 2011. Earliest seafloor hydrothermal systems on Earth: comparison with modern analogues, in: Golding, S.D., Glikson, M. (Eds.), Earliest Life on Earth: Habitats, Environments and Methods of Detection. Springer, Dordrecht, pp. 15–49.

Grabkin, O.V., Mel'nikov, A.I., 1980. The structure of the Siberian Platform Basement in the Marginal-Suture Zone [in Russian]. Nauka, Novosibirsk.

Grichuk, D.V., Lein, A.Yu., 1991. Evolution of the oceanic hydrothermal system and isotope composition of sulfides. Dokl. Akad. Nauk SSSR 318 (2), 422–425.

Grinenko, V.A., Grinenko, L.N., 1974. Geochemistry of Sulfur Isotopes [in Russian]. Nauka, Moscow.

Hulston, J.R., Thode, H.G., 1965. Variations in the S33, S34, and S36 contents of meteorites and their relation to chemical and nuclear effects. J. Geophys. Res. 70 (14), 3475–3484.

Huston, D.L., Brauhart, C.W., Drieberg, S.L., Davidson, G.J., Groves, D.I., 2001. Metal leaching and inorganic sulfate reduction in volcanic-hosted massive sulfide mineral systems: Evidence from the paleo-Archean Panorama district, Western Australia. Geology 29 (8), 687–690.

Ignatiev, A.V., Velivetskaya, T.A., Budnitskiy, S.Y., Yakovenko, V.V., Vysotskiy, S.V., Levitskii, V.I., 2018. Precision analysis of multisulfur isotopes in sulfides by femtosecond laser ablation GC–IRMS at high spatial resolution. Chem. Geology. 493, 316–326.

Jamieson, J.W., Wing, B.A., Farquhar, J., Hannington, M.D., 2013. Neoarchean seawater sulphate concentrations from sulphur isotopes in massive sulphide ore. Nat. Geosci. 6, 61–64.

Johnston, D.T., 2011. Multiple sulfur isotopes and the evolution of Earth's surface sulfur cycle. Earth Sci. Rev. 106 (1–2), 161–183.

Kajiwra, Y., Krouse, H.R., 1971. Sulfur isotope partitioning in metallic sulfide systems. Can. J. Earth Sci. 8, 1397–1408.

Lasaga, A.C., Otake, T., Watanabe, Y., Ohmoto, H., 2008. Anomalous fractionation of sulfur isotopes during heterogeneous reactions. Earth Planet. Sci. Lett. 268, 225–238.

Levchenkov, O.A., Levitskii, V.I., Rizvanova, N.G., Kovach, V.P., Sergeeva, N.A., Levskii, L.K., 2012. Age of the Irkut block of the Prisayan uplift of the Siberian Platform basement: dating minerals from metamorphic rock. Petrology 20 (1), 86–92.

Levitskii, I.V., 2012. Geochemistry of Granulite and Greenstone Complexes of the Cis-Sayan Uplift of the Siberian Platform Basement. PhD Thesis [in Russian]. IGKh SO RAN, Irkutsk.

Levitskii, V.I., 2005. Petrology and Geochemistry of Metasomatism during the Formation of Continental Crust [in Russian]. Akad. Izd. "Geo", Novosibirsk.

Levitskii, V.I., Reznitskii, L.Z., Sal'nikova, E.B., Levitskii, I.V., Kotov, A.B., Barash, I.G., Yakovleva, S.Z., Anisimova, I.V., Plotkina, Yu.V., 2010. Age and origin of the Kitoi sillimanite schist deposit, eastern Siberia. Dokl. Earth Sci. 431 (1), 394–398.

Levitskiy, V.I., Levitskiy, I.V., 2014. Early Precambrian granulite complexes in the South-West of the Siberian Craton, in: Precambrian High-Grade Mobile Belts. Extended Abstracts. Petrozavodsk, pp. 44–45.

Mel'nikov, A.I., 2011. Structural Evolution of Metamorphic Complexes of Ancient Shields [in Russian]. Akadem. Izd. "Geo", Novosibirsk.

Neelov, A.N., 1980. Petrochemical Classification of Metamorphosed Sedimentary and Volcanic Rocks [in Russian]. Nauka, Leningrad.

Ohmoto, H., Goldhaber, M., 1997. Sulfur and carbon isotopes, in: Barnes, H.L. (Ed.), Geochemistry of Hydrothermal Ore Deposits. John Wiley & Sons, New York, pp. 517–611.

Ohmoto, H., Kakegawa, D., Lowe, D.R., 1993. 3.4-billion-year-old biogenic pyrite from Barberton, South Africa: sulfur isotope evidence. Science 262, 555–557.

Ono, S., Eigenbrode, J.L., Pavlov, A.A., Kharecha, P., Rumble III, D., Kasting, J.F., Freeman, K.H., 2003. New insights into Archean sulfur cycle from mass-independent sulfur isotope records from the Hamersley Basin, Australia, in: Earth Planet. Sci. Lett. 213 (1-2), 15–30.

Ono, S., Shanks III, W.C., Rouxel, O.J., Rumble, D., 2007. S-33 constraints on the seawater sulfate contribution in modern seafloor hydrothermal vent sulfides. Geochim. Cosmochim. Acta 71, 1170–1182.

Pavlov, A.A., Kasting, J.F., 2002. Mass-independent fractionation of sulfur isotopes in Archean sediments: strong evidence for an anoxic Archean atmosphere. Astrobiology 2 (1), 27–41.

Peters, M., Strauss, H., Farquhar, J., Ockert, C., Eickmann, B., Jost, C.L., 2010. Sulfur cycling at the Mid-Atlantic Ridge: A multiple sulfur isotope approach. Chem. Geol. 269 (3–4), 180–196.

Petrova, Z.I., Levitskii, V.I., 1984. Petrology and Geochemistry of Granulite Complexes in Cisbaikalia [in Russian]. Nauka, Novosibirsk.

Plyushchev, E.V., Ushakov, O.P., Shatov, V.V., Belyaev, G.M., 1981. Methods of Study of Hydrothermal-Metasomatic Rocks [in Russian]. Nedra, Leningrad.

Poller, U., Gladkochub, D., Donskaya, T., Mazukabzov, A., Sklyarov, E., Todt, W., 2005. Multistage magmatic and metamorphic evolution in the Southern Siberian craton: Archean and Paleoproterozoic zircon ages revealed by SHRIMP and TIMS. Precambrian Res. 136, 353–368.

Predovskii, A.A., 1970. Geochemical Reconstruction of the Primary Composition of Precambrian Metamorphosed Volcanosedimentary Rocks [in Russian]. Kol'skii Filial AN SSSR, Apatity.

Roerdink, D.L., Mason, P.R.D., Farquhar, J., Reimer, T., 2012. Multiple sulfur isotopes in Paleoarchean barites identify an important role for microbial sulfate reduction in the early marine environment. Earth Planet. Sci. Lett. 331–332, 177–186.

Rosen, O.M., 2003. The Siberian craton: tectonic zonation and stages of evolution. Geotectonics, 37 (3), 175–192.

Sal'nikova, E.B., Kotov, A.B., Levitskii, V.I., Reznitskii, L.Z., Mel'nikov, A.I., Kozakov, I.K., Kovach, V.P., Barash, I.G., Yakovleva, S.Z., 2007. Age constraints of high-temperature metamorphic events in crystalline complexes of the Irkut block, the Sharyzhalgai ledge of the Siberian Platform basement: Results of the U–Pb single zircon dating. Stratigr. Geol. Correl. 15 (4), 343–358.

Shabynin, L.I., 1973. Formation of Magnesian Skarns [in Russian]. Nauka, Moscow.

Shen, Y., Buick, R., Canfield, D.E., 2001. Isotope evidence for microbial sulphate reduction in the early Archean era. Nature 410, 77–81.

Turkina, O.M., Sergeev, S.A., Sukhorukov, V.P., Rodionov, N.V., 2017. U–Pb age of zircon from paragneisses in granulite terrane of the Sharyzhalgai uplift (southwest of the Siberian craton): evidence for the Archean sedimentation and evolution of continental crust from Eoarchean to Mesoarchean. Russian Geology and Geophysics (Geologiya i Geofizika) 58 (9), (1281–1297).

Vysotskii, S.V., Ignat'ev, A.V., Velivetskaya, T.A., Levitskii, V.I., Levitskii, I.V., Mekhonoshin, A.S., 2016. Mass-independent fractionation of sulfur isotopes as a tool for solving some problems of petrogenesis of Precambrian ore deposits (by the example of the Cis-Sayan (Sharyzhalgai) marginal uplift of the Siberian craton, in: Geodynamic Evolution of the Lithosphere of the Central Asian Mobile Belt. Proceedings of the Scientific Meeting, Irkutsk, 11–14 October, 2016) [in Russian]. IZK SO RAN, Irkutsk, pp. 43–45.

Wacey, D., McLoughlin, N., Whitehouse, M.J., Kilburn, M.R., 2010. Two coexisting sulfur metabolisms in a ca. 3400 Ma sandstone. Geology 38, 1115–1118.

Wacey, D., Noffke, N., Cliff, J., Barley, M.E., Farquhar, J., 2015. Microscale quadruple sulfur isotope analysis of pyrite from the 3480 Ma Dresser Formation: New insights into sulfur cycling on the early Earth. Precambrian Res. 258, 24–35.

Watanabe, Y., Farquhar, J., Ohmoto, H., 2009. Anomalous fractionations of sulfur isotopes during thermochemical sulfate reduction. Science 324, 370–373.

Whitney, D.L., Evans, B.W., 2010. Abbreviations for names of rock-forming minerals. Am. Mineral. 95, 185–187.

Yudovich, Ya.E., Ketris, M.P., 2000. Fundamentals of Lithochemistry [in Russian]. Nauka, St. Petersburg.

Zharikov, V.A., 1968. Skarn deposits, in: Genesis of Endogenous Ore Deposits [in Russian]. Nedra, Moscow, pp. 220–330.

Editorial responsibility: E.V. Sklyarov